DELFT UNIVERSITY OF TECHNOLOGY

REPORT 13-09

NUMERICAL MODELING OF ROTARY KILN PRODUCTIVITY
INCREASE

M.A. ROMERO-VALLE, M. PISARONI, D. VAN PUYVELDE,
D.J.P. LAHAYE AND R. SADI

Numerical Modeling of Rotary Kiln Productivity Increase

M.A. Romero-Valle[a,*], M. Pisaroni[a], D. Van Puyvelde[b], D.J.P. Lahaye[a], R. Sadi[c]

[a]*Delft Institute for Applied Mathematics, Mekelweg 4, 2628 CD, Delft, The Netherlands*
[b]*Granular Flow Research, 9 Urangarra Place, Jerrabomberra, NSW 2619, Australia*
[c]*Almatis B.V. Theemsweg 30, 3197KM Botlek-Rotterdam, The Netherlands*

Abstract

Rotary kilns are used in many industrial processes ranging from cement manufacturing to waste incineration. The operating conditions vary widely depending on the process. While there are many models available within the literature and industry, the wide range of operating conditions justifies further modeling work to improve the understanding of the processes taking place within the kiln. The kiln being studied in this work produces calcium aluminate cements (CAC).

In a first stage of the project, a CFD empty kiln model was successfully used to counteract ring formation in the industrial partner's rotary kiln. However, that work did not take into account the solids being processed in the kiln. The present work describes the phenomena present within the granular bed of the kiln and links it to the observed productivity increase.

A validated granular bed model is developed taking into account different approaches found in the literature. Simplified sintering reaction kinetics are proposed by considering experimental X-Ray Diffraction data handed by our Industrial Partner and information reported in the literature.

The combined model was used to simulate two sets of operating conditions of the kiln process taking into account the unique chemistry of the calcium aluminates. By combining the aspects of the CFD model for the gas phase and a granular bed model for the solid phase, modeling accuracy is improved and by consequence the phenomena occurring in the kiln are better understood.

Keywords: Rotary Kilns, Computational Fluid Dynamics, MATLAB, Process Modeling

1. Introduction

1.1. Rotary Kilns

Rotary kilns are used in many industrial processes ranging from cement manufacturing to waste incineration. The operating conditions vary widely depending on the process. While there are many models available within the literature and industry, the wide range of operating conditions justifies further modeling work to improve the understanding of the processes taking place within the kiln. The kiln being studied in this work produces calcium aluminate cements.

Rotary kilns are employed to carry out a wide range of operations such as the reduction of oxide ore, the reclamation of hydrated lime, the calcination of petroleum coke and the reclamation of hazardous waste. However, they are much more widely known for their place in the cement industry as the main stage for the manufacture of cement.

---
*Corresponding Author
Current affiliation:
BASF SE
Carl-Bosch-Strasse 38,
67056 Ludwigshafen, Germany
Email addresses: m.a.romerovalle@gmail.com
(M.A. Romero-Valle), michele.pisaroni@gmail.com (M. Pisaroni),
drdennis27@gmail.com (D. Van Puyvelde),
d.j.p.lahaye@tudelft.nl (D.J.P. Lahaye),
rudy.sadi@almatis.com (R. Sadi)
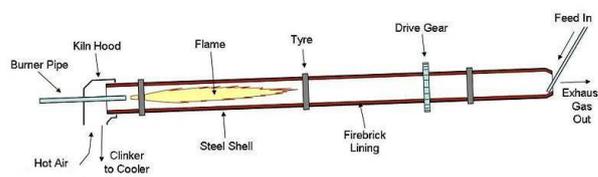
Figure 1: Cement Kiln

A rotary kiln is a pyro-processing device used to raise materials to high temperatures. It is a long horizontal cylinder with a certain inclination with respect to its axis. Material within the kiln is heated to high temperatures so that chemical reactions can take place. A rotary kiln is therefore fundamentally a heat exchanger from which energy from a hot gas phase is transferred to the bed material [3].

Rotary kilns can also be considered as solids chemical reactor, in which one has mainly heat transfer interactions with a gas phase. The phenomena in the solids phase will be addressed with a certain level of detail as it will be the focus of the paper.

1.2. Residence Time and Axial Velocity

The residence time in a rotary kiln is generally dependent on the loading and characteristics of the material in the kiln, the inclination and diameter of the kiln, and the rotating velocity. There are many equations in the literature to predict the residence time. In our case, the residence time is known from

experimental data provided by the Industrial Partner. This residence time and its associated velocity profile is taken as input for the model. The velocity profile assumes a plug flow behaviour of the solid phase in the kiln [3].

1.3. Kiln Fill Geometry
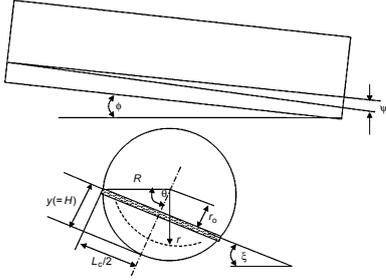
Figure 2: Kiln fill geometry. Note that in this work one assumes a constant fill profile on the kiln, $\Psi \approx 0$ [3]

The definition of kiln load is the percentage of cross sectional area of the kiln which is occupied by the processed granular material. Boateng [3] also mentions that one can make a distinction between a lightly and a heavily loaded kiln. The industrial kiln in question is a lightly loaded kiln. This means that the degree of fill can be assumed as constant along the length of the kiln [3].

1.4. Heat Transfer Phenomena

Brimacombe [4, 5] explains that there are three basic paths of heat transfer into the particle bed:

- The freeboard gas to exposed bed where there are two mechanisms, the radiative heat transfer from the flame and the convective heat transfer from the gases to the bed.

- The exposed wall to exposed bed where there is only one mechanism, the radiative heat reflected from the wall to the bed.

- The covered wall to covered bed where the mechanism is given by conductive heat transfer from the wall to the particle bed.

From all the mechanisms, Boateng [3] mentions that the main path is the radiative heat transfer from flame to the bed. In Figure 3 the basic paths for the heat transfer of a kiln cross section are presented.
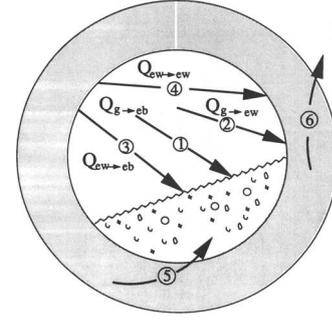
Figure 3: Kiln basic heat transfer paths: 1) Freeboard gas to exposed bed, 2) Freeboard gas to exposed wall, 3) Exposed wall to exposed bed, 4) Exposed wall to exposed wall, 5) Covered wall to covered bed, 6) Loss to surroundings. [5]

1.5. Chemical Reactions

As mentioned in previous sections, the chemical reactions occurring in the studied kiln are sintering reactions. In a sintering process, particles grow and adhere to each other forming different phases [9].

One then can note that the chemical reactions occurring in the kiln can be described as follows:

$$\gamma CaO(s) + \alpha Al_2O_3(s) \rightarrow \gamma CaO \cdot \alpha Al_2O_3(s). \qquad (1)$$

It is to be noted that different phases, resulting from different ratios of eta and gamma of the compounds, occur within different temperature windows. Many of these temperature windows are small which increases the difficulty for operating industrial processes to make these speciality cements.

1.6. Previous Modelling Approaches

There are various approaches in the literature for the modelling of a rotary kiln. All of them make the distinction between two particular phenomena in the kiln, the freeboard phenomena which consists of the gas phase, and the granular bed.

Most of the approaches presented in literature present a CFD approach for the freeboard and a model for the granular bed which deal with chemical reactions and heat exchange [12, 3, 6, 18, 13, 16, 19, 8]. However, there is limited information of industrial applications of such models.

2. Methodology

A model of the kiln wall and granular bed was built using a differential heat balance and solving it with MATLAB. This model was combined with the CFD model developed by Pisaroni [17] to take into account the heat transfer between the flame, kiln wall and kiln charge. The combined model was validated with data from the experimental rotary kiln work by Barr et al [1]. Good agreement was achieved providing confidence in the accuracy of the model.

2.1. Freeboard Model

The CFD Freeboard model developed [17] is a multi-physics model that takes the following phenomena into account: the reactive gas flow and temperature, chemical species and radiative heat transfer distribution in the kiln, the turbulent non-premixed combustion of hydro-carbon gasses in the burner, the insulating properties of the lining, the rotary motion of the kiln and the forced convection on the outside surface.

As the material bed only occupies a small fraction of the volume of the kiln and is assumed to have a negligible impact on the gas phase temperature distribution, one does not take the solids phase into account in the CFD model.

The most important physical phenomenon that takes place on the Freeboard region is the turbulent non-premixed combustion of the fuel injected from the burner with the secondary air. Combustion, even without turbulence, is an intrinsically complex process involving a large range of chemical time and length scales. Some of the chemical phenomena controlling flames take place in short times over thin layers and are associated with very large mass fractions, temperature and density gradients. The modeling of the Freeboard therefore requires resorting to a set of assumptions that are described in the 2012 paper by Pisaroni [17].

2.2. Granular Bed Model

One starts with considering the following assumptions:

- the freeboard gases are perfectly mixed in the transversal direction,

- the granular material has a uniform temperature profile in the transversal plane,

- the granular material flows as a Plug Flow Reactor (PFR) with a mean residence time in the Kiln,

- the granular material is in thermal equilibrium with the freeboard.

For the freeboard gases, homogeneity is questionable due to the fact that in the kiln from the Industrial Partner the burner air injection is not symmetrical. However for the solids, the assumption of homogeneity can be argued as correct due to the low loading of the kiln. The granular flow taken as a PFR is an assumption consequent from the homogeneity of the bed. This is assumed as correct in similar models present in the literature [3, 16, 11, 13].

Lastly, the granular bed is considered to be in thermal equilibrium with the freeboard due to the low loading of the kiln. This assumption is implicit in the approach by Li for Portland Cement Kilns [11].

2.2.1. Governing Equations: Bulk Solids Energy Balance

We consider a differential volume in the bulk solids and do an energy balance:

$$\dot{m}_s c_{p,s} dT_s = q dA \quad [W], \qquad (2)$$

where the left hand side denotes the heating of the bulk material and the right hand side the heat transferred to the material. It is to be noted that the heat transfer paths are the same as described in earlier.

By rearranging the terms we get the following:

$$\dot{m}_s c_{p,s} \frac{dT_s}{dz} = q L_{crd} = \frac{Q L_{crd}}{A} = \frac{Q}{L_K} \quad [Js^{-1}m^{-1}], \qquad (3)$$

where $\dot{m}_s$ is the mass flow rate, $c_{p,s}$ the heat capacity of the solids, T_s the temperature of the bulk solids, q the heat flux into the bulk solids, Q the heat transfer rate, L_{crd} the chord length for calculating the area of heat exchange, A the heat exchange area and L_K the total kiln length.

2.2.2. Radiation

We will present a model for the radiative heat fluxes in the kiln. We use a simplified radiation model presented by Mujumdar [16] in his paper for a one dimensional Portland Cement Kiln model. The following equation is valid for $\varepsilon > 0.8$:

$$Q_{radiation,g \to k} = \sigma A_{g \to k}(\varepsilon_k + 1)\left(\frac{\varepsilon_g T_g^4 - \alpha_g T_k^4}{2}\right) \quad [W], \qquad (4)$$

where the subscript $k = w, s$ represents the gas or the solids phase respectively, σ is the Stefan-Boltzmann constant, A is the area of heat transfer, ε and α are the emissivity and absorptivity of the freeboard gas respectively and T the temperature. This relation is valid for the radiative heat transfer from gas to solids and walls.

We then present the radiative heat transfer from the kiln internal walls to bed given by [16]:

$$Q_{radiation,w \to s} = \sigma A_{w \to s}\varepsilon_s\varepsilon_w\Omega\left(T_w^4 - T_s^4\right) \quad [W], \qquad (5)$$

where Ω is the form factor for radiation which is calculated as follows [16]:

$$\Omega = \frac{L_{scl}}{2(\pi - \xi)R} \quad [-], \qquad (6)$$

where L_{scl} is the length of the chord from the sector covered by the bed, ξ the dynamic angle of repose and R the kiln inner radius. This radiation model is limited to radiation heat transfer from the uncovered wall to the solids bed and from the freeboard to the exposed solids bed.

Lastly, the radiative heat losses from the shell to the environment follows the Stefan Boltzmann Law:

$$Q_{radiation,shell \to ambient} = \sigma A_{w \to s}\varepsilon_{shell}\left(T_{shell}^4 - T_{amb}^4\right) \quad [W], \quad (7)$$

where ε_{shell} is the emissivity of the outer shell and T_{shell} the surface shell temperature.

2.2.3. Convection

There are various correlations for the convective heat transfer from the gas to solids. The selected correlation appears in recent publications for one dimensional models for Portland Cement Kilns by Mujumdar and Li [16, 11]:

$$h^c_{g \to s} = 0.46 \frac{k_g}{D_{eq}} \mathrm{Re}_g^{0.535} \mathrm{Re}_\omega^{0.104} \eta^{-0.341} \quad [W \cdot m^{-2} K^{-1}], \quad (8)$$

where k_g is the gas thermal conductivity and η the kiln load. Re_g and Re_ω are the gas phase and angular Reynolds numbers given by:

$$\mathrm{Re}_g = \frac{u_g D_{eq}}{\nu_g} \quad [-], \quad (9)$$

$$\mathrm{Re}_\omega = \frac{\omega D_{eq}^2}{\nu_g} \quad [-], \quad (10)$$

where u_g is the gas velocity, ν_g the kinematic viscosity of gas and ω the kiln rotational speed [rad/s]. D_{eq} represents the equivalent diameter of the kiln given by [11]:

$$D_{eq} = \frac{0.5D(2\pi - \theta + \sin\theta)}{(\pi - (\theta/2) + \sin(\theta/2))} \quad [m], \quad (11)$$

where D is the internal kiln diameter and θ is the cross-sectional half angle due to the kiln fill as shown in Figure 2.

Similarly, the convective heat transfer coefficient from gas to internal walls is calculated by:

$$h^c_{g \to w} = 1.54 \frac{k_g}{D_{eq}} \mathrm{Re}_g^{0.575} \mathrm{Re}_\omega^{-0.292} \quad [W \cdot m^{-2} K^{-1}], \quad (12)$$

which has the same nomenclature as Equation 8.

The previously presented heat transfer coefficient correlation was developed by Tscheng and Watkinson [3] experimentally and validated with data from the available literature.

Finally, the convective heat transfer coefficient between the outer wall and environment when $Re_w / \sqrt{Gr} \geq 0.2$ is calculated from [11]:

$$h^c_{sh \to a} = \frac{k_a \mathrm{Pr}^{0.3}}{D} \left(\mathrm{Re}_a^2 + 0.5 \mathrm{Re}_\omega^2 + Gr \right)^{0.35} \quad [W \cdot m^{-2} K^{-1}], \quad (13)$$

where k_a is the thermal conductivity of the air, Pr is the Prandtl number, D is the outer diameter of the kiln, Re_a the Reynolds number of the ambient air, Re_ω the rotational Reynolds number and Gr the Grashof number given by:

$$Gr = \frac{g\beta(T_{shell} - T_{amb})D^3}{\nu^2} \quad [-], \quad (14)$$

where g is the acceleration due to gravity, β the volumetric thermal expansion coefficient from air, T_{shell} the shell surface temperature, ν the kinematic viscosity of air and D the outer diameter of the kiln.

Similarly, we have for $Re_w / \sqrt{Gr} < 0.2$ [11]:

$$h^c_{sh \to a} = \frac{k_a \mathrm{Pr}^{0.3}}{D} C \mathrm{Re}_a^N, \quad (15)$$

where N is the revolutions per minute and C a correction factor, which in the present model is used to adjust heat losses to match the measured values from the plant.

2.2.4. Wall to Bed Heat Transfer

As Boateng and Li remark on their publications [3, 11] there are a number of correlations for the wall to bed heat transfer coefficients. The heat transfer coefficient developed by Li [11] is selected due to the fact that it is based in physical phenomena:

$$h_{w \to s} = \left(\frac{\chi d_p}{k_g} + \frac{0.5}{\sqrt{2k_b \rho_b c_{pb} n/\phi}} \right)^{-1} \quad [W \cdot m^{-2} K^{-1}], \quad (16)$$

where d_p denotes the particle diameter, k_g the thermal conductivity of the gas, k_b the thermal conductivity of the bulk solids, ρ_b the bulk density, $c_{p,b}$ the heat capacity of the bulk solids, n the r.p.m. of the kiln and ϕ the central half angle. Additionally, χ can take a value between 0.096 - 0.198 and denotes the thickness of the gas layer between the solids and the walls. This correlation has been validated with data from industrial Portland Cement Kilns and pilot-scale kiln data from literature [11].

2.2.5. Material Physical Properties

The physical properties for the gas and solids are calculated with existing correlations reported in literature [3, 11, 16]. However, for the bulk solids one has to take into account the void fraction of the material by averaging the solid and gas properties as follows:

$$\Phi_{eff} = e\Phi_{gas} + (1 - e)\Phi_{solid} \quad [-], \quad (17)$$

where Φ corresponds to the physical property i.e., conductivity, emissivity, and so on, and e corresponds to the solid void fraction.

For the thermal conductivity and diffusivity of the bulk solids we use the following expressions presented by Boateng which takes radiation into account [3]:

$$k_b = \frac{1 - e}{\frac{1}{k_s} + \frac{1}{4\sigma\varepsilon d_p T^3}} + e4\sigma\varepsilon d_p T^3 \quad [W \cdot m^{-1} K^{-1}], \quad (18)$$

$$\alpha_b = \frac{k_b}{\rho_b c_{p,s}} \quad [m^2 \cdot s^{-1}], \quad (19)$$

where e is the void fraction, k_s the thermal conductivity of the solids, σ the Stefan Boltzmann constant, ε the emissivity of the solids, d_p the diameter of the particles, T the temperature of the bulk solids, ρ_b the density of the bulk solids, $c_{p,s}$ the specific heat of the bulk solids and α_b the thermal diffusivity of the bulk solids.

It is important to note that most physical properties such as heat capacity, density, conductivity and so on, are dependent on the temperature. The expressions for such properties can be found in literature.

2.2.6. Mathematical Model

Then by considering the heat transfer correlations shown above, the heat balance of the bulk solids reads as follows:

$$\dot{m}_s c_{p,s} \frac{dT_s}{dz} = \frac{1}{L_K}\left[\sigma A_{g\to s}(\varepsilon_s + 1)\left(\frac{\varepsilon_g T_g^4 - \alpha_g T_s^4}{2}\right)\right]$$
$$+ \frac{1}{L_K}\left[h_{g\to s}A_{g\to s}(T_g - T_s) + h_{w\to s}A_{w\to s}(T_w - T_s)\right], \tag{20}$$
$$[Js^{-1}m^{-1}]$$

where in addition to the nomenclature described in the previous sections we have T denoting temperature, A area of heat exchange and the subscripts s, g, and w denoting the bulk solids, gas and wall respectively.

We need an additional equation due to the unknown wall temperature. We then solve the energy balance across the kiln walls:

$$Q_{gas\to wall} + Q_{radiation,gas\to wall} - Q_{wall\to solids} -$$
$$Q_{radiation,wall\to solids} = Q_{shell\to ambient} \quad [W]. \tag{21}$$

where $Q_{shell\to ambient}$ denotes the heat losses from the shell of the kiln to the environment. Then by using Newtoń law of cooling we get the following:

$$Q_{shell\to ambient} = UA_{shell}(T_w - T_{amb}) \quad [W], \tag{22}$$

where A_{shell} is the outer area of the steel shell of the kiln, T_w is inner wall temperature, T_{amb} the ambient temperature and U_{shell} is the overall heat transfer coefficient given by [2]:

$$U_{shell} = \frac{1}{\frac{\log(R_{lin}/R_{in})}{k_{lin}2\pi L} + \frac{\log(R_{out}/R_{lin})}{k_{steel}2\pi L} + \frac{1}{h_{sh\to amb}^c}} \quad [W \cdot m^{-2}K^{-1}], \tag{23}$$

where R is the radius, k the thermal conductivity, L the length of the section and $h_{sh\to amb}^c$ the convective heat transfer coefficient between the kiln outer wall and the environment.

2.3. Chemical Reactions

The reactions occurring in the kiln are of the following form:

$$\gamma CaO(s) + \eta Al_2O_3(s) \to \gamma CaO \cdot \eta Al_2O_3(s). \tag{24}$$
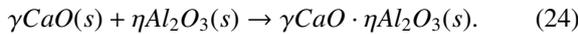
Given available X-Ray diffraction data for the same molar ratio of CaO and Al_2O_3 used by the industrial partner on its industrial kiln, and using data such as the activation energy present in literature, a simplified reaction model taking only into account the conversion of alumina is developed.

One can describe the rate of a solid-state reaction by the following Arrhenius type equation [10]:

$$\frac{dX_A}{dt} = A_e e^{-(E_a/RT)} f(X_A), \tag{25}$$

where A_e is the pre-exponential factor, E_a the activation energy, T the absolute temperature, R the universal gas constant,

$f(X_A)$ the reaction model and X_A the conversion fraction of alumina.

Assuming the reaction being controlled by diffusion as described in [7, 15], the Ginstling-Brounshtein (D4) model is selected which is given for the differential form [10] as:

$$D_4(X_A) = f(X_A) = 3\left[2((1 - X_A)^{-1/3} - 1)\right]^{-1}, \tag{26}$$

where X_A is the conversion fraction of alumina as in Equation 25. This reaction model was developed for diffusion controlled reactions in three dimensions.

It is to be noted that the experimental data available is non-isothermal, thus we make use of the heating rate which is also available and we then have:

$$\frac{d\alpha}{dT} = \frac{A}{\beta} e^{-(E_a/RT)} f(X_A), \tag{27}$$

where β is the heating rate (dT/dt).

Using the X-Ray diffraction data from the Industrial Partner, and information such as the activation energy present in literature, it is proceeded to adjust Equation 25 by varying the pre-exponential factor A_e. An activation energy of $E_a = 205$ kJ/mol is selected, corresponding to the primary phase of the product manufactured by the Industrial Partner. By iterating and taking the best fit, the exponential factor has the value $A_e = 14500$ s^{-1}.
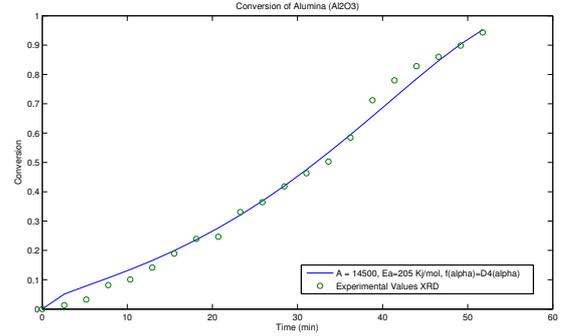
Figure 4: Conversion vs. Time, $R^2 = 0.997$

Then Equation 20 is modified and one includes the heat of reaction (ΔH^{rxn}):

$$\dot{m}_s c_{p,s} \frac{dT_s}{dz} = Q_{radiation,g\to s} + Q_{convection,g\to s}$$
$$+ Q_{conduction,w\to s} + \dot{n}_A \Delta H^{rxn}, \tag{28}$$

where $\dot{n}_A$ is the moles of A consumed per unit length (dn_A/dz).

One defines the heat of reaction as $\Delta H^{rxn} = 30$ kJ/mol, an average of the material produced by the Industrial Partner. One then has the following:

$$\frac{dn_A}{dz} = x_{A,0} \frac{\dot{m}_s}{Mw_A} \frac{dt}{dz} \frac{dX_A}{dt} =$$
$$x_{A,0} \frac{\dot{m}_s}{Mw_A} \frac{\bar{\tau}}{L_K} A e^{-(E_a/RT)} D_4(X_A), \tag{29}$$

5

where $x_{A,0}$ is the molar fraction of alumina at the feed of the kiln, $\dot{m}_s$ the mass flow of the solids, Mw_A the molecular weight of alumina, $\bar{\tau}$ the residence time of the kiln and L_K the length of the kiln.

It is to be noted that the simplified model only takes into consideration the conversion of alumina. It does not take into account side reactions and intermediates which are known to occur.

2.4. Solution Procedure

First, the temperature field calculated from the freeboard CFD model is processed to have a 1-D average freeboard gas temperature. Then one solves Equations 22, 28 and 29 with MATLAB [14] using the ODE and DAE solver "ode15s". Note that the system of equations to be solved is a Differential Algebraic System (DAE).

As parameters, one can modify the initial feed temperature of the material bed, the outer steel shell heat transfer coefficient and environmental temperature and gas temperature at the discharge.

Due to the high process temperatures, temperature dependent material properties were used such as the Shomate equations for heat capacity.

2.5. Validation

To validate the model, experimental work from Barr et al. was used [1]. The paper from Barr aims to provide pilot kiln data for the verification of heat-transfer models. It considers experiments with an inert bed and with calcination reactions. Run T4 from the mentioned paper will be used due to the fact that it is an experiment with an inert bed. The geometry and operating conditions of the kiln used for the experimental work from Barr are described in Table 1.

Geometry		Operating Conditions		Properties	
L_K	5.5 (m)	n	1.5 (rpm)	k_b	0.27 (W/m k)
D_K	0.406 (m)	$\dot{m}_s$	17 (g/s)	ρ_s	1650 (kg/m^3)
η	12% (-)	U_g	2 (m/s)		

Table 1: Data from Barr et al. [1] used in the bed model validation
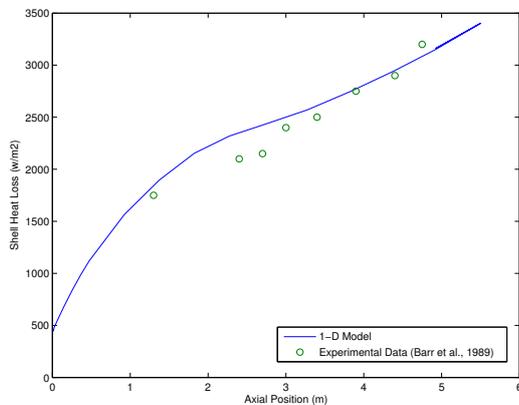
Figure 5: Outer Shell Heat Loss [1]

In addition to the data described in the previous table, data from other one-dimensional models was used for the freeboard and lining [3, 11, 16]. In order to calibrate the model, the experimental results of the heat flux at the outer shell were matched with the results from the model by varying the outer shell convective heat transfer coefficient of the model. We can observe in Figure 5 the match obtained with respect to the heat flux at the outer shell.

One then can observe in Figure 6 good matching between our 1-D model and the experimental results from Barr et al [1]. It is to be noted that the experiment run analyzed was done without chemical reactions.
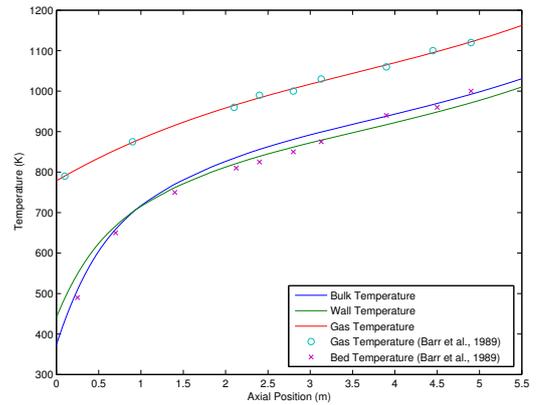
Figure 6: Temperature Profiles of the 1-D model and run T4 from Barr et al. [1]

These results indicate that the model described in the previous section is valid for rotary kilns with an inert bed. Furthermore, it can be inferred that for the kiln to be analyzed the model is also valid as reaction kinetics are derived and validated with data from the Industrial Partner.

3. Results

The combined model was used to simulate two sets of operating conditions of the kiln process taking into account the unique chemistry of the specialty cement. To calibrate the model, temperature measurements were done on the kiln outer shell. Furthermore, the outer shell heat losses were matched similar to what was done on the validation section.

With the standard operating conditions, the model showed the hot spot as indicated by the previous CFD modeling efforts [17]. However, the addition of the granular bed model allowed the conversion of the bed material to be estimated as well as the proportion of the material in the kiln that was in the liquid state. This is shown in Figure 7 for the standard operating conditions of the kiln. As previously reported, the kiln was subject to producing rings and the location of the ring coincides with the high proportion of the liquid state in the kiln.
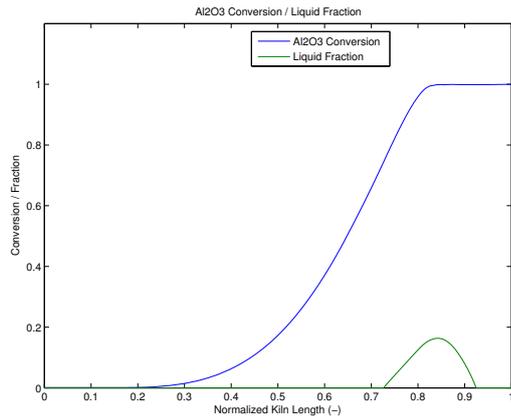
Figure 7: Conversion vs Kiln Length, Standard Operating Conditions

Figure 7 also shows that with standard conditions full conversion of alumina is achieved with 80% of the kiln length. This can be translated into wasted energy input at the last 20% of the kiln length and a possibility of side reactions occurring after full conversion. The previous assertion can be supported by observations made by the Industrial Partner in which for standard operating conditions product quality was not optimal.

The Industrial Partner changed their operating conditions to reduce the ring formation [17]. They reported a better quality of product when the operating conditions were optimized for ring removal compared to their standard operating conditions. One can infer that the discrepancies in product quality between the mentioned cases may be due to the possibility of side reactions occurring after the raw material achieves full conversion and higher proportion of melt, as shown in Figure 7. This contrasts the optimized operating configuration, which has a slower conversion and lower melt fraction, as shown in Figure 8.
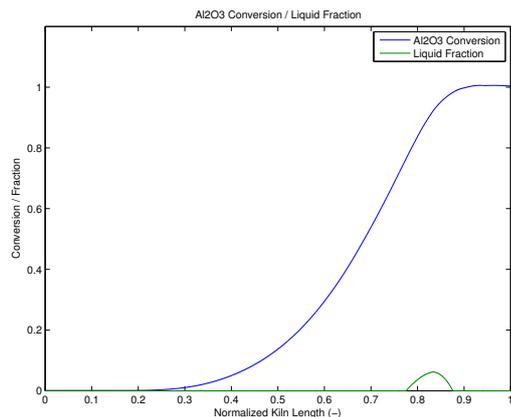
Figure 8: Conversion vs Kiln Length, Optimized Operating Conditions

By having a better product quality, the Industrial Partner has less off-spec material discarded from the process. Additionally by having a lower proportion of clinker melt, the ring formation is reduced which in turn means less down-time for the kiln and lower maintenance costs as described previously in[17]. The
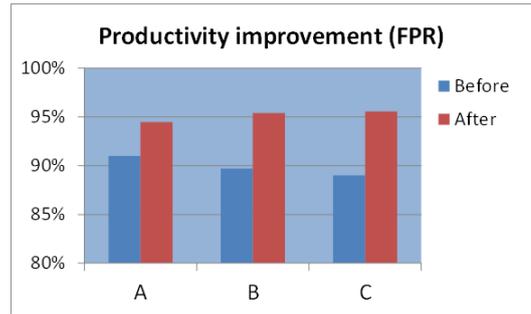
Figure 9: Productivity of Products A, B and C, before and after the optimization of operating conditions [2]

consequences of having better quality and a better operation is translated into a productivity increase as reported by the Industrial Partner in Figure 9.

The model not only provides a better understanding of the phenomena occurring in the kiln, but also gives insight on the reason of the observed productivity increase.

4. Conclusions

As the combined model effectively explains the observed behavior of the studied kiln, it may be used to evaluate further kiln configuration changes. The model is currently used for the evaluation of process parameter changes in order to reduce energy consumption and NOx emissions.

The application of CFD and granular bed modeling allows improved model quality and better understanding of industrial processes. It can be used to effectively solve practical problems that industry faces daily, in turn maximizing profitability for industry.

5. Further Work

Any modelling work always depends on a range of assumptions made throughout the development of the model. The fundamentals of this model are based on well understood CFD models and residence time observations of the granular bed. Additional work could be carried out to improve the complexity of the reaction kinetics of the solids to better represent a complete set of reaction kinetics. This could produce better insights on the concentration profiles of the granular bed but also more exact estimations of the temperature profile and the clinker melt as the different solid phases have different liquidus and solidus temperatures. Any modelling work could also be further improved by additional calibration with data from operating kilns.

References

[1] P. Barr, J. Brimacombe, and A. Watkinson. A heat-transfer model for the rotary kiln: Part i. pilot kiln trials. *Metallurgical and Materials Transactions B*, 20:391–402, 1989. 10.1007/BF02696991.

[2] R.B. Bird, W.E. Stewart, and E.N. Lightfoot. *Transport phenomena*. Wiley International edition. J. Wiley, 2007.

[3] A.A. Boateng. *Rotary kilns: transport phenomena and transport processes*. Chemical, Petrochemical & Process. Elsevier/Butterworth-Heinemann, 2008.

[4] J.K. Brimacombe and A.P. Watkinson. Heat transfer in a direct-fired rotary kiln: 1. pilot plant and experimentation. *Metallurgical Transactions*, 9B:201–208, 1978.

[5] J.K. Brimacombe and A.P. Watkinson. Heat transfer in a direct-fired rotary kiln: 2. development of the cross-section model. *Metallurgical Transactions*, 20B:403–419, 1989.

[6] Michael David Heydenrych. *Modelling of Rotary Kilns*. PhD thesis, Universiteit Twente, 2001.

[7] Suketoshi Ito. Layer formation and apparent activation energies of formation of calcium aluminates. *Zeitschrift fuer Physikalische Chemie*, 1977.

[8] Ursula Kääntee. Modelling a cement manufacturing process to study possible impacts of alternative fuels. *Extraction and Processing Division Meeting on Recycling and Waste Treatment in Mineral and Metal Processing: Technical and Economic Aspects*, 2002.

[9] S.J.L. Kang. *Sintering: densification, grain growth, and microstructure*. Materials science & engineering. Elsevier Butterworth-Heinemann, 2005.

[10] Ammar Khawam and Douglas R. Flanagan. Solid-state kinetic models: Basics and mathematical fundamentals. *The Journal of Physical Chemistry*, 110(35):17315–17328, 2006. PMID: 16942065.

[11] S.-Q. Li, L.-B. Ma, W. Wan, and Q. Yao. A mathematical model of heat transfer in a rotary kiln thermo-reactor. *Chemical Engineering & Technology*, 28(12):1480–1489, 2005.

[12] F. Marias. A model of a rotary kiln incinerator including processes occurring within the solid and the gaseous phases. *Computers & Chemical Engineering*, 27(6):813 – 825, 2003.

[13] E Mastorakos, A Massias, C.D Tsakiroglou, D.A Goussis, V.N Burganos, and A.C Payatakes. Cfd predictions for cement kilns including flame modelling, heat transfer and clinker chemistry. *Applied Mathematical Modelling*, 23(1):55 – 76, 1999.

[14] MATLAB. version 7.14.0 (r2012a). The MathWorks Inc., 2012.

[15] Beshir Mohamed and John H. Sharp. Kinetics and mechanism of formation of monocalcium aluminate. *J. Mater. Chem.*, 7(8), 1997.

[16] K.S. Mujumdar and V.V. Ranade. Simulation of rotary cement kilns using a one-dimensional model. *Chemical Engineering Research and Design*, 84(3):165 – 177, 2006.

[17] M Pisaroni, R Sadi, and D Lahaye. Counteracting ring formation in rotary kilns. *Journal of Mathematics in Industry*, 2(1):3, 2012.

[18] Matthias Schumacher Uwe Küssel, Dirk Abel and Martin Weng. Modeling of rotary kilns and application to limestone calcination. *Proceedings 7th Modelica Conference, Como, Italy*, pages 20–22, 2009.

[19] Shijie Wang, Jidong Lu, Weijie Li, Jie Li, and Zhijuan Hu. Modeling of pulverized coal combustion in cement rotary kiln. *Energy & Fuels*, 20(6):2350–2356, 2006.